Microporous and Mesoporous Materials 219 (2016) 219–229

Contents lists available at ScienceDirect

Microporous and Mesoporous Materials

journal homepage: www.elsevier.com/locate/micromeso

SBA-15 mesoporous silica highly functionalized with propylsulfonic pendants: A thorough physico-chemical characterization

Alice Silvia Cattaneo [a], Chiara Ferrara [a], Davide Carlo Villa [a], Simone Angioni [a], Chiara Milanese [a], Doretta Capsoni [a], Stefania Grandi [a], Piercarlo Mustarelli [a], Valentina Allodi [b], Gino Mariotto [b], Sergio Brutti [c], Eliana Quartarone [a, *]

[a] Department of Chemistry and INSTM, University of Pavia, Via Taramelli 16, I-27100 Pavia, Italy
[b] Dept. of Informatics, University of Verona, Strada Le Grazie 15, I-37134 Verona, Italy
[c] Dept. of Science, University of Basilicata, Viale dell'Ateneo Lucano 10, I-85100 Potenza, Italy

ARTICLE INFO

Article history:
Received 20 May 2015
Received in revised form
6 July 2015
Accepted 10 August 2015
Available online 19 August 2015

Keywords:
Mesoporous silica
SBA-15
Functionalization
Solid-state NMR

ABSTRACT

Organosulfonic modified SBA-15 silicas are promising catalysts for a wide spectrum of organic reactions. In particular, their catalytic activity seems to be effective only when large amounts of functional groups are anchored to the silica skeleton. However, there is evidence that the ordered mesostructure is retained only for contents of sulfonic units not exceeding 20 mol%.

In this paper, for the first time to our knowledge, we fully address the gradual structural disordering mechanisms of the SBA-15 silica functionalised with increasing amounts of propylsulfonic groups in the compositional range 0–70 mol%. This investigation was carried out by means of a multi-technique wide approach including thermal analysis, TEM, XRD, N_2 adsorption, FTIR/Raman and solid-state multinuclear NMR.

We obtained detailed information on the structural modifications of these hybrid systems as a consequence of the sulfonation process. In particular, we showed that high functionalization degrees lead to inhomogeneous materials made of inorganic or low-functionalized clusters where the SBA-15 structure is likely retained, and hybrid clusters where the hexagonal mesoporous structure is destroyed. Moreover, full conversion of –SH into $-SO_3H$ groups is efficient until 20 mol% functionalization. In fact for higher sulfonation degrees, the formation of S–S bridges becomes a competitive mechanism, which is predominant in the sample SO3H70%, where only about 20% of the introduced organic moieties are actually oxidized. Therefore, to push sulfonic functionalization above 20 mol% is not necessarily useful, at least for applications where ordered mesoporous structure is mandatory, such as in catalysis or in membranes for polymer fuel cells.

1. Introduction

The discovery of hexagonally-ordered mesoporous silicas was one of the most striking novelties in 90's materials chemistry, due to the exciting potentiality of such systems [1–5]. They show, in fact, extremely high surface area and homogeneous and geometrically well-defined pores. The pores dimensions may be easily and properly modulated at the nanoscale by changing the synthesis conditions and, in particular, by choosing suitable templates. Thanks to these peculiar morphological properties, novel architectures of porous nano-reactors can be designed, which find applications in several technological fields including catalysis [6–10], nanomedicine [11,12], optics [6,13], environment [14,15] and energetic [16].

In order to further improve the performances of the ordered mesoporous silica-based systems and to overcome some important limitations, mostly in terms of stability and reactivity, a number of organic–inorganic hybrid materials were prepared by incorporating different functional groups onto the silica surface [4–7,15–18]. As a matter of fact, organic functionalization of mesoporous silica is a route to introduce or modulate important surface properties, such as hydrophilicity or hydrophobicity, reactivity, host–guest interactions, chemical resistance, and other functional performances (mechanical, optical, electric, etc.) [6,7,9].

* Corresponding author.
E-mail address: eliana.quartarone@unipv.it (E. Quartarone).

http://dx.doi.org/10.1016/j.micromeso.2015.08.011
1387-1811/

Among the various mesoporous silicas, SBA-15 is considered a model system for many possible functionalizations [4,6,7,17], because it combines unique morphological features (e.g. high surface area and porosity, thick pore walls) with high thermal [3,19] and mechanical stability [20]. In fact, SBA-15 consists of a regular one-dimensional hexagonal array of mesopores with a well-defined narrow pore size distributions, peaked between 3 and 4 and 30 nm, depending on the template used during the synthesis.

Among the huge variety of possible reactive moieties considered for the sake of functionalization, one of the most investigated groups is indeed the sulfonic one (−SO_3H), which allows the hybrid silica to act as a solid acidic catalyst in chemical conversion of large molecules, so representing an effective alternative to the traditional homogeneous systems, namely H_2SO_4, HF, $AlCl_3$, BF_3 [4,21]. In spite of some interesting results, however, the catalytic activity of SBA-15 with sulfonic groups is not yet competitive with respect to H_2SO_4. One of the reasons for this could be the too low amount of SO_3H-moieties anchored to the porous skeleton. This prompted to seek for higher functionalization degrees. Recently, Xiao et al. synthesized mesoporous silica functionalized with a nominally high number of sulfonic moieties, and tested their catalytic activity in the esterification reaction of cyclohexanol with acetic acid. They observed a progressive improvement of the esterification yields by increasing the sulfonation level. In particular, similar conversion degrees were obtained by comparing the silica containing 80 mol% of propylsulfonic groups with concentrated H_2SO_4 (92% and 96.5%, respectively) [21].

Alkylsulfonic-functionalized mesoporous silica can be usually prepared by two methods: i) silylation of the preformed inorganic solid and subsequent SH-oxidation [5,22]; ii) co-condensation of TEOS and mercaptopropyltrimethoxysilane (MTPMS) as the precursors via a template route. The thiol groups are subsequently oxidized by a post-synthesis H_2O_2 acidification to give −SO_3H units [4,16,21,23].

The latter synthesis approach presents several advantages, the most important one being that it allows a more homogeneous distribution and a higher degree of functionalization of the inorganic skeleton. For these reasons, it was widely used and further optimized by performing a direct oxidative approach, which allowed to obtain a periodic sulfonated mesostructure, with surface area and pores volume higher than those obtained by post-synthesis oxidation. This strategy also led to better acid exchange capacities, typically ranging between 1 and 2 meq of H^+/g of SiO_2, which make such systems more performing in terms of catalytic performances. This synthesis involves the one-step reaction between TEOS and MTPMS, in presence of Pluronic® as the template, in HCl and H_2O_2 as the oxidant agents, so allowing the in-situ conversion of the thiol groups to the sulfonic ones [4].

However, only a low content of sulfonic groups (up to 20 mol%) seems to be actually compatible with the ordered mesostructure typical of these materials. A more extended oxidative process aimed at increasing the functionalization degree, in fact, seriously sacrifices the periodic mesoporosity, by altering the characteristic uniform nano-channels, and dramatically decreases the surface area and the pore volume [21]. Some improvements in this sense could be reached by controlling the synthetic conditions, for instance the surfactant nature [21,23,24], but a better understanding of the structural modification occurring during the functionalization steps could be particularly helpful, both in the optimization of the synthetic processes of these hybrid materials, and in the quest for obtaining very high functionalization degrees (ideally above 50 mol%).

Aim of the present work is to investigate, by means of a multi-technique approach, the structure of both low and high sulfonic-functionalized mesoporous silicas, in order to systematically explore the modifications induced by the organic functionalization into the silica network. Hybrid silicas with −SO_3H content ranging between 10 and 70 mol% were prepared by a one-step synthesis, similar to that already described in literature [4], and widely characterized using X-ray powder diffraction, nitrogen adsorption, TEM, thermogravimetry, vibrational (FT-IR/Raman) and solid-state NMR spectroscopies. In particular, the latter technique is a very useful tool for the structural investigation of inorganic–organic hybrid materials, as it gives important insights of the local structure in the sub-nanometer scale [17,18,25–28].

2. Experimental

2.1. Synthesis of mesoporous SBA-15 silica

Mesoporous SBA-15 silica was synthesized by means of a template-based sol–gel procedure, as reported by Zhao in 1998 (see Scheme 1) [3]. In a typical synthesis, 2 g of the template agent Pluronic 123®, was dissolved with stirring in 62.5 g of 1.9 M HCl at room temperature. The solution was heated at 40 °C before adding 4.5 g (0.0216 mol) of tetraethylorthosilicate (TEOS). The mixture was first maintained at 40 °C for 20 h under stirring, then was aged at 100 °C for 24 h under static conditions in a sealed vessel. The obtained solid product was filtered, washed with distilled water and then with ethanol. In order to remove the template, a calcination at 550 °C for 6 h in air was performed as the final step.

2.2. Synthesis of sulfonic functionalized silica samples

The hybrid SBA-15-type silicas containing sulfonic groups were synthesized by a one-step process involving a co-condensation of TEOS and a thiosilane precursor in presence of an oxidizing agent, namely H_2O_2, as already reported in the literature [4] and sketched in Scheme 2.

As for the SBA-15, 2 g of Pluronic 123® was first dissolved in 62.5 g of 1.9 M HCl at room temperature and the solution was subsequently heated at 40 °C before adding TEOS. After 40 min at the same temperature, the thiol precursor, mercaptopropyltriethoxysilane (MPTMS), and a concentrated solution of hydrogen peroxide (2 mL, 30 wt%) were successively added. The molar amounts of TEOS and MPTMS were properly chosen in order to obtain nominal degree of functionalization ranging between 10 and 70 mol% (see also Table 1). For instance in the case of silica with a degree of 50% of functionalization the solution was obtained adding 0.0108 mol of TEOS (2.25 g, 2.4 mL) and 0.0108 mol of MPTMS (2.12 g, 2.0 mL). The obtained mixture was stirred at 40 °C for 20 h and then aged at 100 °C for 24 h under static conditions in a sealed vessel. The obtained suspension was then centrifuged for 10 min at 6000 r.p.m. and the solid product recovered by filtration, washed several times with ethanol and rinsed with distilled water. The silica was allowed to dry in air at room temperature overnight, and

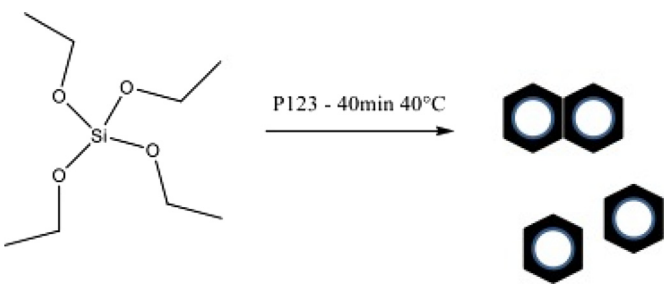

Scheme 1. Synthesis of hexagonal mesoporous SBA-15 silica.

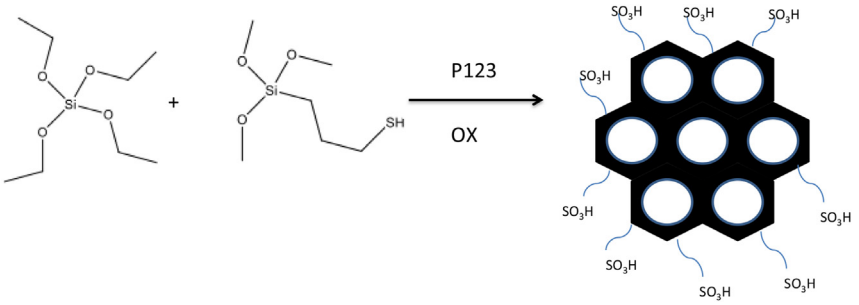

Scheme 2. Synthesis of functionalized SBA-15-type silicas.

Table 1
Z Potential and microstructural parameters of the functionalized samples: surface area (S), pore volume (V_p) and pore size ($d_{p,BJH}$) obtained from N_2 adsorption measurements (pore size calculated on the basis of the BJH approach); d (100) and wall thickness (a_0-d_p, where $a_0 = 2(d(100))/3^{1/2}$ is the lattice parameter) obtained by means of XRD analysis. n: narrow, w: wide; from TGA: wt_{H20} = loss of adsorbed water, wt_{R1} = loss of mercaptopropyl groups, wt_{R2} = loss of the propylsulfonic groups.

Sample	−SO_3H mol% (nominal)	S (m^2/g)	V_p (cm^3/g)	$d_{p,BJH}$ (Å)	d (100) (Å)	Wall thickness (Å)	Z potential (mV)	wt_{H20} (%)	wt_{R1} (%)	wt_{R2} (%)
SBA-15	–	744	1.4	65	93.8	43.3	3.5	0.4	–	–
SO3H10%	10	736	1.0	50	94.0	58.5	−16.2	1.1	4.5	13.3
SO3H20%	20	707	0.95	40	98.6	73.9	−17.3	1.5	5.6	14.1
SO3H50%	50	600	0.79	40, n 120,w	–	–	−19.9	2.7	8.7	25.6
SO3H70%	70	199	0.39	40, n	–	–	−23.4	3.8	8.9	27.9

then the template was removed from the as-synthesized material by washing with ethanol under reflux for 48 h (1.5 g of as-synthesized material per 400 mL of ethanol). In the case of silica with functionalization degrees higher than 50 mol%, a second oxidation step was necessary to complete the conversion of thiol groups to the sulfonic ones. After the solvent extraction, 1 g of silica was treated with 100 mL of a solution of hydrogen peroxide (15 wt %) and acetic acid (1 wt%) for 1 h at 40 °C. The silica was finally filtered and washed with a solution of sodium metabisulphite in water (20 wt%), and then rinsed several times with distilled water. The final product was dried under vacuum overnight.

2.3. Physico-chemical characterization

N_2 adsorption/desorption isotherms were obtained by means of a Thermo Electron Sorptomatic 1990 instrument on samples previously dried at 150 °C under vacuum (10^{-3}/10^{-4} atm) for 8 h. Adsorption data were analyzed by the conventional Brunauer, Emmett and Teller (BET) method [29], whereas desorption data were treated by means of Barrett, Joyner and Halenda (BJH) approach [30], in order to analyze the pore size distributions and specific pore volume even in case of larger pores (up to 300 nm).

A Malvern Zetasizer Nano ZS90 was employed to investigate the surface charge of the particles (Z-Potential). The powder was dispersed in water (0.2 mg/mL). Each sample solution was loaded into disposable cuvettes.

The vibrational properties of pure and sulfonated silica specimens were investigated by both FT-IR and micro-Raman spectroscopies. FT-IR spectra of the powder embedded in KBr pellets were obtained in transmission configuration using a JASCO spectrometer (FT/IR-660 plus) equipped with a Tri-Glycine-Sulfate (TGS) detector. All the IR spectra were recorded in the spectral range between 400 and 4000 cm^{-1} with a resolution of 4 cm^{-1}, and a polystyrene film was used as the wavenumber reference. A proper baseline was carefully subtracted from each FT-IR spectrum in the aim to ensure a reliable analysis. Micro-Raman spectroscopy measurements between 400 and 3200 cm^{-1} were carried out at room temperature in backscattering geometry using a micro-sampling set-up (Horiba-Jobin Yvon, model Labram HR) consisting of a He–Ne laser as the excitation source (632.8 nm), a 80 cm focal length single-monochromator and a notch filter for the Rayleigh line cut-off. The scattered radiation was dispersed by a diffraction grating having 600 lines/mm and detected at the spectrograph output by a multichannel detector, a CCD with 1024 × 256 pixels, cooled with liquid nitrogen. The spectra were obtained by focusing the laser beam through a 100× objective, with a numerical aperture close to 1. The laser power at the samples surface was kept below 5 mW. All the spectra were calibrated in wavenumber using the emission lines of an Ar spectral lamp. Repeated micro-Raman spectra were carried out under the same experimental conditions from different micro-regions of the investigated sample, in order to verify the spectra reproducibility over the sample surface. The recorded spectra were processed to remove artefacts due to cosmic rays, while the luminescence background was subtracted before starting the analysis of the experimental data.

The thermogravimetric measurements were performed in a Q5000 equipment (TA Instruments). For each sample, about 10 mg of powder were equilibrated in a Pt crucible under N_2 flow at 35 °C for 1 h for removing humidity, and then heated up to 850 °C at 5 °C/min.

X-ray powder diffraction (XRD) measurements were performed using a Bruker D5005 diffractometer with the CuKα radiation, graphite monochromator and scintillation detector. The patterns were collected with a step size of 0.02° and counting time of 6 s per step in the angular range 0.8–2.9°.

Solid-state NMR spectra were obtained on a Bruker Avance III 400 MHz spectrometer based on a 9.4 T magnet. ^{29}Si MAS NMR spectra were acquired in a 7 mm MAS probe operating at the spinning speed of 5 kHz. For quantitative single pulse experiments, a 90° pulse of 11 μs and a recycle delay of 300 s were used. The recycle delay was chosen after a T_1 inversion recovery measurement performed on pure SBA-15, obtaining a $T_1 = 58 \pm 1$ s for the Q^4 site. ^{29}Si (^1H) CP MAS experiments were recorded using: ^1H 90° pulse of 4.2 μs, contact time of 3 ms, spinal.64 decoupling scheme and recycle delay of 5 s. Chemical shifts are reported relative to TMS, using tetrakis(trimethylsilyl)silane as secondary standard,

with $\delta = -9.8$ ppm for the trimethylsilyl groups. ^{13}C and ^{1}H MAS NMR spectra were acquired in a 4 mm MAS probe operating at the spinning speed of 11 kHz. ^{13}C single pulse experiments were acquired using a 90° pulse of 4.6 μs, a recycle delay of 30 s and spinal.64 decoupling. $^{13}C(^{1}H)$ CP MAS experiments were acquired using: ^{1}H 90° pulse of 4.2 μs, contact time of 2.5 ms, spinal.64 decoupling scheme and recycle delay of 5s. ^{1}H one pulse experiments were recorded using a 90° pulse of 4.2 μs, and a recycle delay of 20 s. For both the nuclei chemical shifts are reported relative to TMS, using adamantane as secondary standard. The spectra were fitted to Gauss/Lorentz curves, using the DMFIT program [31].

Transmission electron microscopy experiments were carried out with a FEI G2 20 HR-TEM instrument equipped with a LaB_6 electron beam source and two 2D flat cameras (low resolution and high resolution) at 200 kV e-beam acceleration. Samples were suspended in hexane in ultrasonic bath (5 cycles of 15 min of ultrasonic treatment followed by 45 min of rest to cool down the sample and thus avoid thermal heating), and dispersed on copper holey carbon film grids for observation. Image analyses were carried out by using the ImageJ software [32,33].

3. Results and discussion

As already stated in the previous sections, samples of SBA-15-type silica modified with propylsulfonic groups were prepared by means of a one-step synthesis by varying the nominal molar fraction of $-SO_3H$ units, *X*, between 10 and 70 mol%. The $-SO_3H$ molar ratio, *X*, is defined as the molar fraction of the silane precursor with respect to the total amount of condensation co-reagents, as per the following equation (1):

$$X\ (\%) = \frac{n_{MPTMS}}{(n_{MPTMS} + n_{TEOS})} \quad (1)$$

Table 1 reports the nominal molar compositions, *X*, chosen for the investigated samples. The actual ones, calculated through the analysis of the ^{29}Si NMR spectra, are reported in Table 2. The content of the functionalizing groups effectively incorporated into the silica network quite fairly agrees with the nominal ones (average discrepancy ~16%). This confirms that the synthetic process was successful even for high functionalization degrees. However, these data are referred to the presence of organic units anchored to the silica backbone. The actual conversion to sulfonic groups was estimated indirectly by means of thermogravimetry, surface charge measurements and more directly through spectroscopic investigations, as discussed below.

3.1. TGA analysis

Fig. 1a–d shows the TGA thermograms and the respective DTG curves collected in the temperature range between 35° and 850 °C for all the sulfonated silica samples. Prior of the scan, the samples were maintained for 1 h in N_2 flow in order to remove moisture adsorbed on the surface. The plots of pure SBA-15 (e) are also reported for the sake of comparison. As better evidenced by the DTG curves, three main steps of weight change can be easily identified, whose values are reported in Table 1. The first one, up to 100 °C, is due to the desorption of water, which increases with the $-SO_3H$ molar content due to the enhanced hydrophilicity caused by the presence of more acidic moieties. Water contents of about 3% and 4% are, in fact, measured in case of both 50% and SO3H70%, respectively (see Table 1). The other ones are due to the decomposition of the organic groups anchored to the silica network. They occur in the temperature range 250–500 °C and they actually consist of two consecutive phenomena, one above 250 °C, and the other one at T > 450 °C, which are correlated to the decomposition of the mercaptopropyl- and propylsulfonic groups, respectively [4]. We will show in the following by means of FT/Raman and NMR spectroscopies that it is possible to exclude the presence of unreacted SH-moieties in all samples, and the less stable sulfur-containing species have to be identified as disulfide and thiosulfonate bridges. As show both by TGA curves and Table 1, the degradation of the $-SO_3H$ moieties takes place in the same temperature range for all the samples and, as expected, the entity of the weight loss increases proportionally with *X*. In contrast, the onset of the step involving the other sulfur-containing groups starts at lower temperature in case of higher functionalization, suggesting that highly functionalized systems do present a wider range of organic species (see also ^{13}C MAS NMR, Section 3.8).

3.2. Z-potential analysis

The presence of acidic moieties on the SBA-15 surface could be qualitatively confirmed by measuring the space charge by Z potential analysis. Table 1 reports the Z Potential values obtained at room temperature vs. the SO_3H-functionalization degree on colloids prepared by properly dispersing the silica samples in water. As expected, in presence of incorporated acidic groups, the Z potential of SBA-15-type organosilicas becomes negative due to the dissociation of SO_3H-units, which originate a negatively charged surface of the particles. The Z values, and then the colloidal stability, slightly increase with the content of organic sulfonic groups, and values higher than −20 mV are reached in presence of $-SO_3H$ molar fraction above 50 mol%.

3.3. Vibrational dynamics analysis

Raman spectra of pure SBA-15 show five main peaks at 486, 604, 786, 825 and 980 cm^{-1} (see Fig. 2). The SBA-15 spectrum is similar to the pure silica one, with the exception of the intensity of the peak at 980 cm^{-1}, by far more relevant in the mesoporous system, in

Table 2
Assignment and quantification of the different silicon species from ^{29}Si MAS NMR.

Si site	δ_{CS} (ppm, ± 0.2)	Silicon site quantification (%, ±0.2)				
		SBA-15	SO3H10%	SO3H20%	SO3H50%	SO3H70%
T^2	−58.2	–	1.1	5.0	12.6	11.2
T^3	−66.7	–	6.5	11.9	31.1	49.4
Q^2	−92.0	5.1	3.3	4.6	2.4	2.1
Q^3	−101.3	36.3	26.3	25.8	18.7	11.0
Q^4	−110.6	58.6	62.8	52.7	35.2	26.3
		Q^2: Q^3: Q^4 (%)				
		5: 36: 59	3: 28: 69	6: 31: 63	4: 33: 63	5: 28: 67
		$T^m/(T^m + Q^n)$ (%)				
		–	8 ± 2	17 ± 2	44 ± 5	61 ± 8

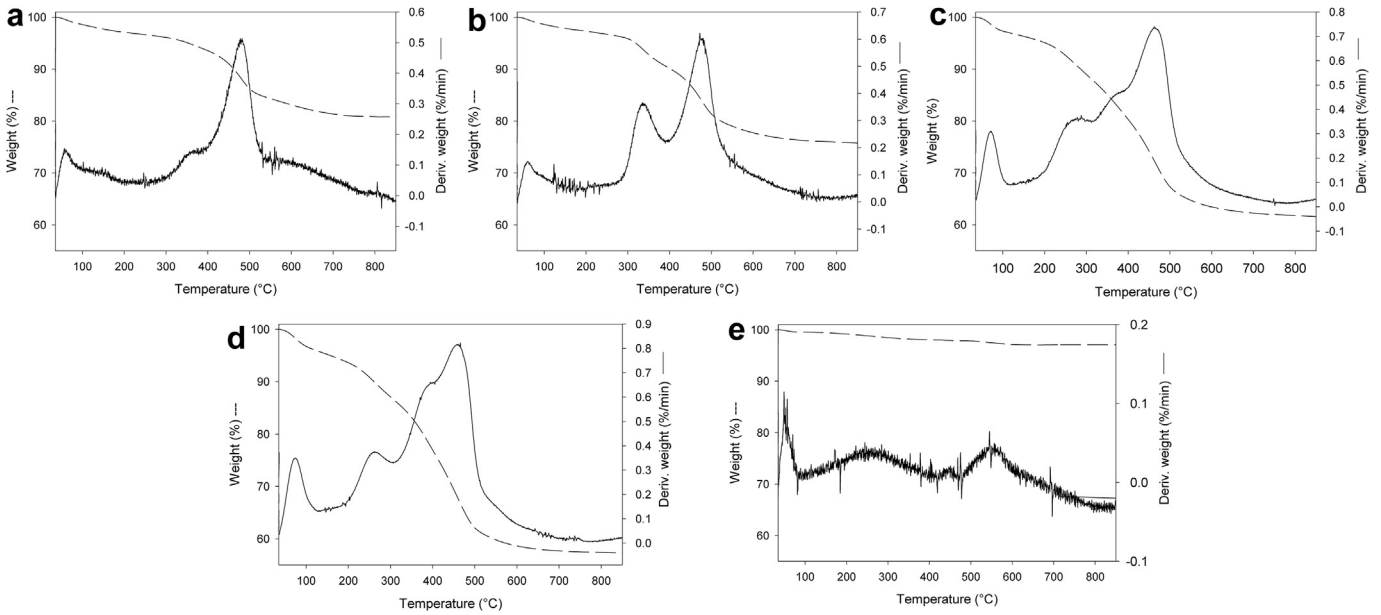

Fig. 1. SBA-15 (e), and propylsulfonated samples: SO3H10% (a), SO3H20% (b), SO3H50% (c), and SO3H70% (d).

fairly good agreement with the literature [34]. Likewise it occurs in silica, the two peaks at 795 and 825 cm^{-1} are due to the vibration of siloxane bridges, whereas the peaks at 486 and 604 cm^{-1} are related to the vibrations of four and threefold siloxane rings and the peak at 980 cm^{-1} is attributed to surface silanol groups [35]. New spectral features appear in the Raman spectra of functionalized samples: in fact, three peaks due to CH_2 stretching modes are visible in the higher energy region at about 2895, 2934 and 2978 cm^{-1}, while the two new peaks at 1045 cm^{-1} and 1119 cm^{-1} are due to symmetric and antisymmetric vibrational modes of the SO_3^- groups. Moreover, other peaks occur between 1300 and 1460 cm^{-1}, probably due to deformation of CH_2 groups. Furthermore, the band at 980 cm^{-1} is shifted toward lower wavenumbers (until to reach 967 cm^{-1} in the case of heavily functionalized samples), as already observed in literature for similar SBA-15-type silica functionalized by means of other reactive moieties [34].

As far as concerns the FT-IR investigations, the absorption spectra shown in Fig. 3 corroborate the Raman results: for pure SBA-15, the four peaks, occurring respectively at 465, 803, 967 and 1090 cm^{-1}, are attributed to silica modes [36], while the remaining two bands are due to bending (around 1700 cm^{-1}) and stretching (at about 3400 cm^{-1}) of water. In the functionalized samples, the peak at 967 cm^{-1} shifts to lower frequency (down to 958 cm^{-1}), while both the SO_3^- and CH_2 modes appear and become more and more evident when the propylsulfonic content increases. In fact, besides the CH_2-stretching peak at about 2900 cm^{-1}, the SO_3^- symmetric and antisymmetric vibrational modes are clearly visible at 1046 and 1125 cm^{-1}, respectively (see Fig. 4). In both Raman and FT-IR spectra no evidence of residual non-reacted SH-moieties was found, in particular due to the absence of SH-stretching peak at around 2600 cm^{-1} [37].

3.4. N_2 adsorption/desorption measurements

The mesostructural properties of the SBA-15 based materials were investigated by means of the N_2 adsorption isotherms obtained for the pure SBA-15 and the functionalized samples, SO3HX% (X = 10–70 mol%) (see Supplementary Information). Such curves are classified as belonging to the IV type, as expected in case of

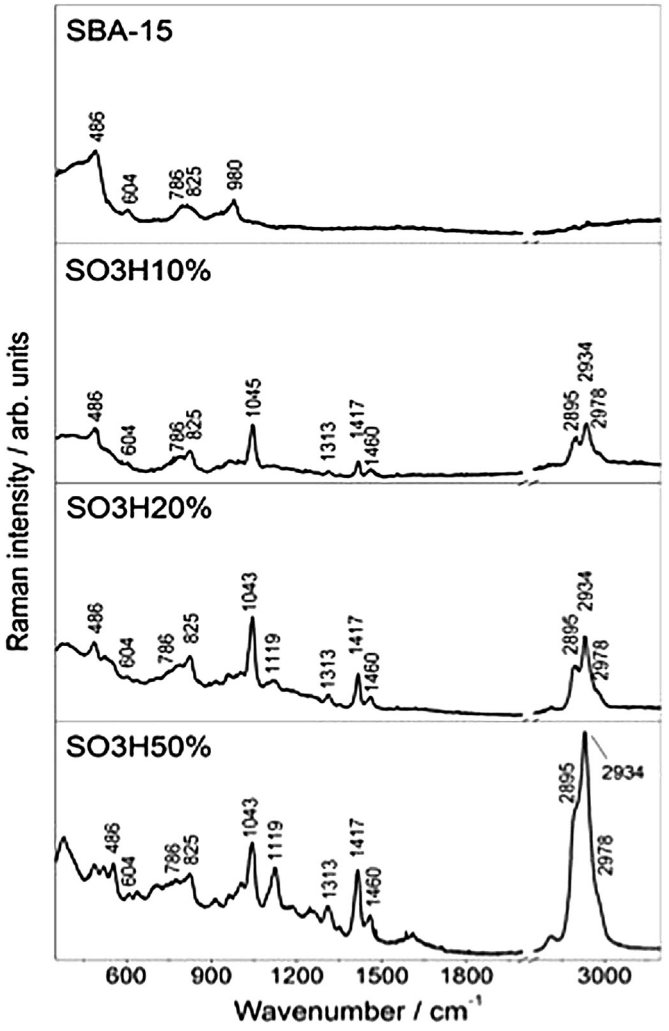

Fig. 2. Raman spectra of pure SBA-15 (top panel) and functionalized SBA-15-type silica samples.

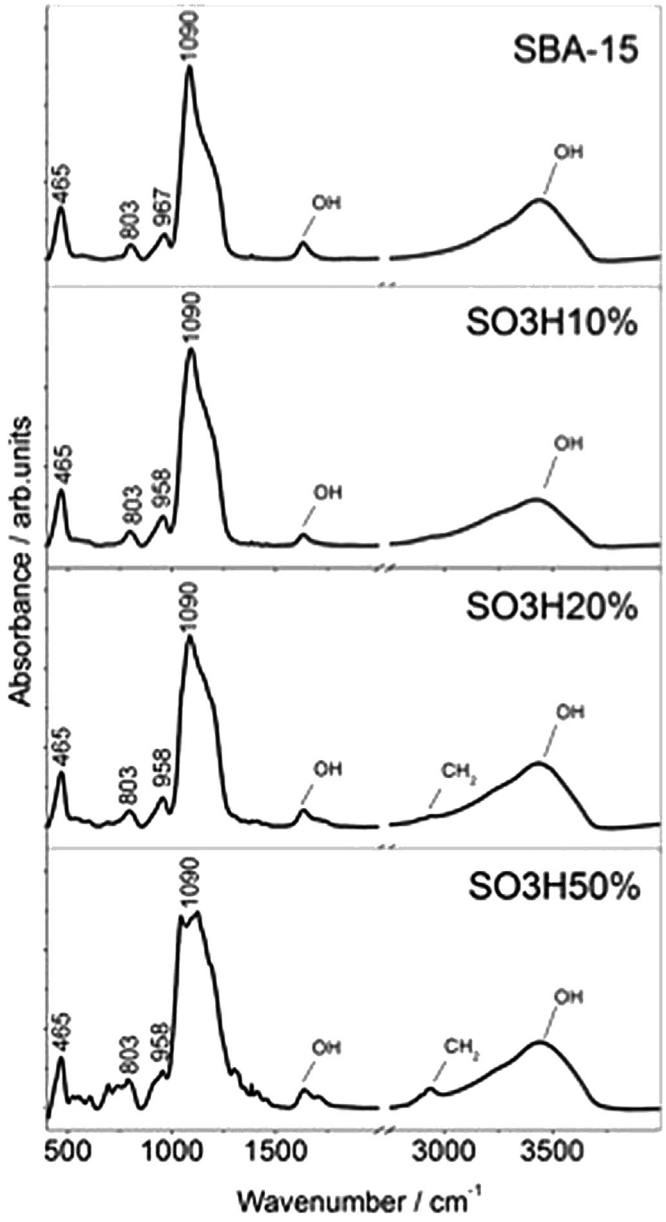

Fig. 3. FT-IR spectra of pure SBA-15 and functionalized SBA-15-type silicas, recorded in transmission mode.

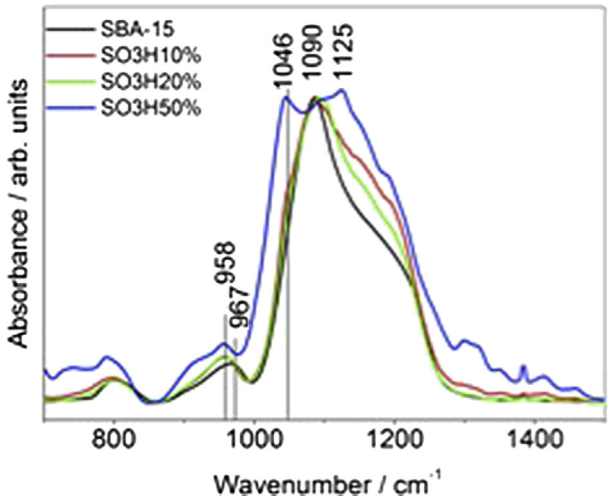

Fig. 4. FT-IR spectra of pure and functionalized SBA-15-type silica samples, in the spectral region 700–1500 cm^{-1}.

mesoporous solids, i.e. they show the typical hysteresis loop which is usually associated with the capillary condensation in mesostructures. However, the shape of the hysteresis curves is remarkably affected by the nature of the silica samples, which is generally identified by the specific pore structures. From the analysis of the plots, we observe that the pure SBA-15 shows a H1-type loop, where the adsorption and desorption branches are almost parallel and vertical over a wide range of relative pressure, p/p_0. Such branches appear quite sharp, similar to what reported in literature, suggesting a narrow pore size distribution [38]. In contrast, the functionalized systems tend to give H2-type loops [39], which become more and more pronounced by increasing the content of $-SO_3H$ moieties. A H2-type shape, in particular, indicates a not well-defined distribution of pore size and shape. The capillary condensation occurs at p/p_0 of about 0.6 only for the pure SBA-15 and SO3H10%. When the content of the sulfonic groups increases, this phenomenon occurs at lower relative pressure (p/p_0 ~0.5). The position of the adsorption branch is related to the pore size distribution; in particular, capillary condensation pressure is an increasing function of the pore diameter. Such curves then suggest that the pore size tend to decrease with the increase of sulfonic functionalization. Table 1 reports the pore sizes corresponding to the pore size distribution (PSD) maxima, obtained using the Barrett–Joyner–Halenda (BJH) model [29]. The pore size distribution is mono-modal with a sharp maximum between 6 and 7 nm for SBA-15 and SO3H10%. For higher content of organic groups, the size of the pores decreases in the range 3–4 nm, and for SO3H50% a bimodal distribution is observed, which is characterized by a narrow peak centered between 3 and 4 nm and by a wide peak between 9.5 and 13.5 nm. The shrinking of the silica pore dimensions also results in a gradual reduction of both BET specific surface area and total pore volume, as reported in Table 1, which definitively indicates an important reduction of the mesoporous structure of samples with a functionalization degree higher than 20 mol%, in agreement with X-ray diffraction and TEM results.

3.5. XRD analysis

Fig. 5 shows the low angle, X-ray powder diffraction patterns of the pristine SBA-15 and the sulfonated samples (up to 50 mol%). SBA-15 shows three peaks which are indexed as the (100), (110) and (200) reflections of the typical *p6mm* hexagonal structure, of this mesoporous silica [4]. The same peaks are also observed for the SO3H10% and SO3H20% samples, but a shift towards lower angles and an intensity decrease by increasing the functionalization degree can also be noted. These evidences indicate that, up to 20%, the hexagonal symmetry is preserved and the a_0 unit–cell parameter increases by increasing the functionalization degree. In fact, the $d(100)$ spacings for SBA-15, SO3H10% and SO3H20% are 93.8, 94.0 and 98.6 Å respectively, corresponding to unit cell parameter values a_0 of 108.3, 108.5 and 113.9 Å. This can be translated into well defined wall thickness values, which increase with the $-SO_3H$ molar fraction from 43 Å to 74 Å (see Table 1). A similar evidence was previously observed by Xiao et al., who attributed this phenomenon to the adopted synthesis conditions involving a fluorocarbon–hydrocarbon surfactant mixture as the template [21]. The enhancement of the wall thickness should be indeed interpreted in terms of structural changes during the single step condensation, which are induced by the higher amounts of organic

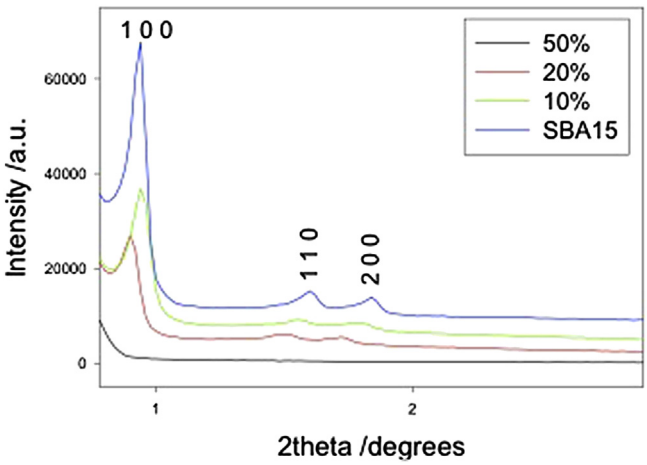

Fig. 5. XRD patterns of SBA-15 and SO3HX% (X = 10–50 mol%) samples.

moieties anchored to the inorganic skeleton. The SO3H50% sample shows a completely different XRD pattern. No diffraction peaks are observed, suggesting that the hexagonal mesoscopic organization is not yet preserved.

3.6. TEM

Fig. 6 shows the transmission electron micrographs of the synthesized materials, both bare and functionalized. As expected, the pristine SBA-15 material shows a well defined and ordered mesoporosity with highly parallel channels (Fig. 6A) [3]. Low magnification TEM images (not shown here), suggest irregular round-like primary particles of approximately 300–500 nm in diameter with regular linear channels extended along the entire particle. The morphologies of the sulfonated silica materials are altered if compared to the pure SBA-15. An increase of the functionalization degree corresponds to a progressive morphology evolution. Apparently, the SO3H10% and SO3H20% samples still show a residue of ordered mesoporosity in the core of the primary particles, whereas their surfaces result to be more defective (Fig. 6B and C). As already observed in the XRD analysis section (see Table 1), the wall thickness of the functionalized mesoporous silicas seems to increase with the functionalization degree. In fact, passing from the pure silica to the SO3H10% and SO3H20% samples, it is possible to estimate from TEM images wall thicknesses values of 31 ± 10, 47 ± 6 and 57 ± 5 Å, respectively. Besides the differences in the estimated absolute values between XRD and TEM, the increasing trend is confirmed by both techniques. On the other hand, the pore diameters show a reverse decreasing trend. The mean channel size estimated from TEM images results to be 49 ± 12 and 36 ± 6 Å for the SO3H10% and SO3H20% samples, respectively, in excellent agreement with the BJH analysis of the nitrogen adsorption data (see Table 1). In contrast, the SO3H50% material (Fig. 6D) shows a drastic and extended alteration of the morphology. There is a total loss of ordered mesoporosity, and the sample shows a homogeneous amorphous-like morphology, extending from the surface to the core of the primary particles.

3.7. ^{29}Si MAS NMR

The extent of the MPTMS incorporation into the silica materials can be monitored through solid state NMR spectroscopy, which provides a deep investigation of the microstructural evolution of the prepared samples [4]. The quantitative ^{29}Si single pulse NMR spectra acquired for pure SBA-15, and the propylsulfonic functionalized silicas SO3H10%, SO3H20%, SO3H50%, and SO3H70% are reported in Fig. 7. The spectra can be interpreted in terms of Q^n and T^m sites. Q^n terms refer to $[Si(OSi)_n(OH)_{4-n}]$ with n = 0, 1, 2, 3, 4 units and thus identify the possible siloxane species, while T^m terms are referred to $[RSi(OSi)_m(OH)_{3-m}]$ units, defining the Si species which are bonded to an organic moiety. Q^n and T^m sites are characterized by different chemical shift ranges of −80 to −120 ppm and −50 and −80 ppm, respectively [40]. The spectrum of pure SBA-15, in agreement with previous literature [3,4], is characterized by the presence of three distinct signals at −92, −101 and −110 ppm, related to Q^2, Q^3 and Q^4 species, respectively. The Q^4 signal is due to the $[Si(OSi)_4]$ units, the fundamental building blocks of the material bulk, which are located into the thick silica walls. The Q^2 and Q^3 species, presenting one and two −OH groups respectively, are mainly located on the silica surface and the edges of the pores [4,17,41]. The spectrum of the propylsulfonic-functionalized samples shows two additional peaks at −58 ppm and −67 ppm, which are ascribed to T^2 and T^3 sites, respectively. The predominance of T^3 over T^2 species confirms that the MPTMS precursor is effectively condensed as a part of the silica framework [42]. The total amount of T^n species monotonically increases with the increase of the MPTMS/TEOS ratio. By the evaluation of the integrals, it is possible to estimate the actual ratio $T^m/(T^m + Q^n)$, which can be compared with the expected functionalization grade [4,17,41]. The obtained values are in good agreement with the nominal compositions.

It was already shown that until 20 mol% functionalization [4], the Q^n sites distribution remains similar to that showed by pure SBA-15, suggesting a retention of the SBA-15 mesoporous framework. At higher degrees of organic functionalization, as in the samples SO3H50% and SO3H70%, we could expect a progressive modification of the peculiar SBA-15 structure, presumably leading to a marked change in the Q^2: Q^3: Q^4 ratios and to an increase of Q^2 units located in defect sites. In fact, the MPTMS precursor is not able to form four Si–O–Si bonds, which are the fundamental building block for the formation of the hexagonal SBA-15 cell. However, it can be observed that the pattern in the Q^n units range remains similar in all samples as far as concerns the line width, which is related to local disorder. Moreover, the Q^2: Q^3: Q^4 ratio doesn't change dramatically for increasing functionalization, and no clear trend can be observed (see Table 2). The scenario described from these NMR data is not compatible with a homogeneous distribution of the organic groups with increasing functionalization. In fact, such a distribution should lead to an average increase of local defects into the silica network. The relative small changes into the ^{29}Si spectra recorded for the highest functionalized samples, both in terms of peaks internal ratio and lineshape pattern, suggest an inhomogeneous distribution of the organic pendants, which locally gives origin to almost inorganic or low-functionalized clusters where the SBA-15 structure is retained, and to clusters (dominant by increasing functionalization) where the hexagonal mesoporous structure is destroyed. This naïve picture can explain the bimodal pore distribution obtained from the N_2 adsorption isotherms, as well as the loss of long-range mesoporosity stated by XRD patterns for the SO3H50% and SO3H70% samples.

3.8. ^{13}C MAS NMR

Additional information on the organic functionalization with the increasing amount of MPTMS/TEOS ratio is obtained by using ^{13}C MAS NMR. Fig. 8 shows both the $^{13}C(^1H)$ CP MAS and single pulse MAS experiments recorded for silica samples with up to 70 mol% functionalization. The SO3H10% sample shows three main peaks, which can be attributed to propylsulfonic chains. The signals at 53 and 18 ppm represent the methylene carbons in α and β

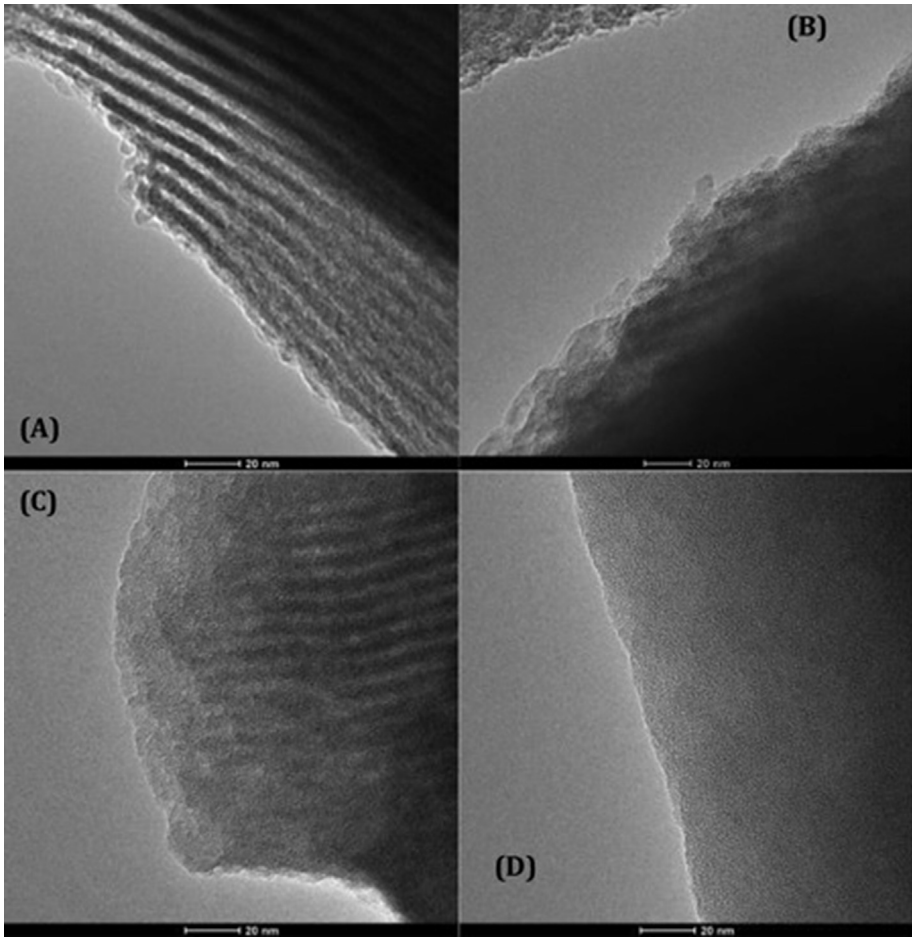

Fig. 6. TEM micrographs of SBA-15 (A), SO3H10% (B), SO3H20% (C), and SO3H50% (D) samples.

positions of the $-SO_3H$ moiety, while the peak at 11 ppm can be assigned to the CH_2 unit near Si. The absence of signals at 27 and 22 ppm, corresponding to CH_2 in α and β to a −SH moiety, suggests the complete oxidation of the thiol groups to $-SO_3H$ [4,42–44], in agreement with the vibrational spectroscopy results. The remaining additional peaks can be ascribed to a small residual amount of copolymer template [4,45] and ethanol into the pores (see Table 3). Due to their high mobility inside the mesoporous cavities, their signals are hardly recognizable into the $^{13}C(^{1}H)$ CP MAS NMR spectrum (see Fig. 8a). The spectrum recorded for the silica functionalized at 20 mol% (SO3H20%) resembles that obtained for SO3H10%, but two new contributions in the 50–20 ppm range can also be observed. These peaks have to be assigned to disulfide bridges ($Si(CH_2)_3S–S(CH_2)_3Si$), arising from the condensation of two mercaptopropyl chains. The signals at about 41 and 23 ppm correspond to methylene carbons in α and β positions, respectively [42,43]. The same secondary byproduct can be also observed in the higher functionalized silica samples (Fig. 8b). In the spectrum obtained for the SO3H50% sample, we found evidences also of a second byproduct: a thiosulfonate moiety $Si(CH_2)_3S–S(O_2)–(CH_2)_3Si$, produced by the partial oxidation of disulfide bridges. In fact, the peak at 64 ppm is attributed to CH_2 carbons near $S(O_2)$, whereas the broad signal centered at 39 ppm can be described as the overlapping of two contributions of methylene in α to either S–S or $S–S(O_2)$ moieties (38 and 41 ppm, respectively). The same byproducts are also found in the SO3H70% sample. In its spectrum, moreover, also residual traces of the templating agent can be found.

In all the samples, signals clearly attributable to unreacted mercaptopropyl groups were not observed, so demonstrating that the chosen oxidation conditions are enough for a complete conversion of the −SH moiety to $-SO_3H$. However, already a MPTMS-functionalization of 20 mol% led to the formation of cyclic byproducts with disulfide or/and thiosulfonate bridges. The coexistence of the two byproducts was already reported by several groups, even at low functionalization levels, if a small amount of H_2O_2 was employed for the −SH to $-SO_3H$ conversion [43,44]. In our samples the formation of S–S bridges is indeed a competitive mechanism, which becomes progressively dominant with an increasing amount of mercaptopropyl moiety. It is useful to note that in case of SO3H50% and SO3H70% samples also a post-oxidation after the one-pot synthesis was performed. We suggest that part of the S–S bridges underwent oxidation to $S–S(O_2)$ during this step.

Our experiments allowed us also to make a rough estimation of the ratio between propylsulfonic moiety and disulfide bridges, by considering the ratio between the integration area of the peaks ascribed to the methylene carbons in α position to the different moieties (53, 39, 41 and 64 ppm, see Table 3 for single assignments). At 10 mol% functionalization, all the mercaptopropyl groups were oxidized into propylsulfonic groups, whereas at 20 mol% already 40% are involved in disulfide bridges. In the SO3H50% sample still half of the mercaptopropyl groups are converted into $-SO_3H$ moiety. The most functionalized sample, SO3H70%, showed a poor conversion of SH to sulfonic moieties, in fact just 10–20% of the entire mercaptopropyl groups has been

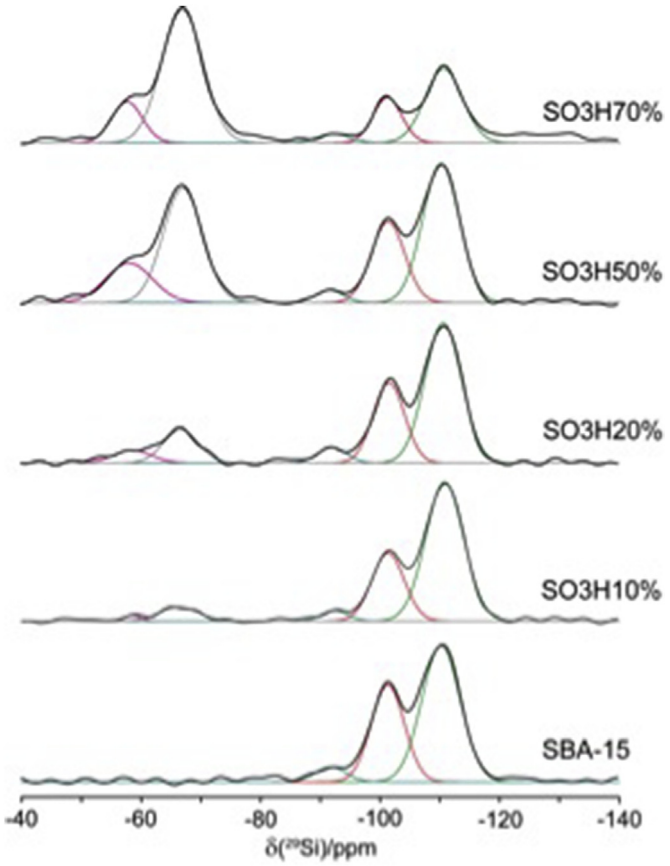

Fig. 7. ^{29}Si quantitative single pulse MAS NMR spectra recorded for pure SBA-15 and several propylsulfonic functionalized mesoporous silicas. The colored lines are line-shape deconvolution components summarized in Table 2.

effectively converted. This massive amount of disulfide bridges probably hinders the correct formation of both the hierarchical and the local order into the SBA-15-like silica network in SO3H70%, confirming that its ^{29}Si NMR spectrum, where the SBA-15 typical Q^3/Q^4 ratio seems to be retained (see Fig. 7), can be explained only in terms of sample inhomogeneity. As already stated, this sample likely contains a non-random distribution of the organic chains, but there are still small domains where TEOS condensed to form a SBA-15-like network, excluding any organic moiety. This hypothesis is further corroborated by the relatively poor signal-to-noise ratio for both ^{13}C(^{1}H) CP MAS and one-pulse experiment, which suggests that the organic content could be less than expected.

3.9. ^{1}H MAS NMR

For the same series also ^{1}H MAS NMR spectra were acquired (see Fig. 9 and Table 4 for peak assignments). In pristine SBA-15 the water coordinated with the silanol groups located both into the pores and on the surface does resonate at about 5 ppm, where also the H-bonded silanols fall [46]. The sharp peaks at 3.7 and 1.1 can be attributed to residual copolymer template [41,47] and ethanol. In the SO3H10% sample, a part of the water interacts with the sulfonic groups. As a result, the broad signal at 6.6 ppm accounts also for the sulfonic acid protons, which are under chemical exchange with protons from water molecules, as already demonstrated in previous studies [10,41]. The signal assigned to Pluronic® can be found also in this sample. In the range 4–0 ppm three signals ascribed to the propylsulfonic chains can be observed: 3.2, 1.5 and 0.4 ppm arising from the methylene protons in α, β, and γ positions to $-SO_3H$, respectively [10]. A similar spectrum was recorded for SO3H20%, but the signals accounting for water and sulfonic acid protons resulted to be markedly narrower, probably due to a lower amount of H-bonds between water and the silanols. The SO3H50% shows a spectrum with a main peak centered around 7.4 ppm and a complex overlapping of many peaks forming a broad and featureless

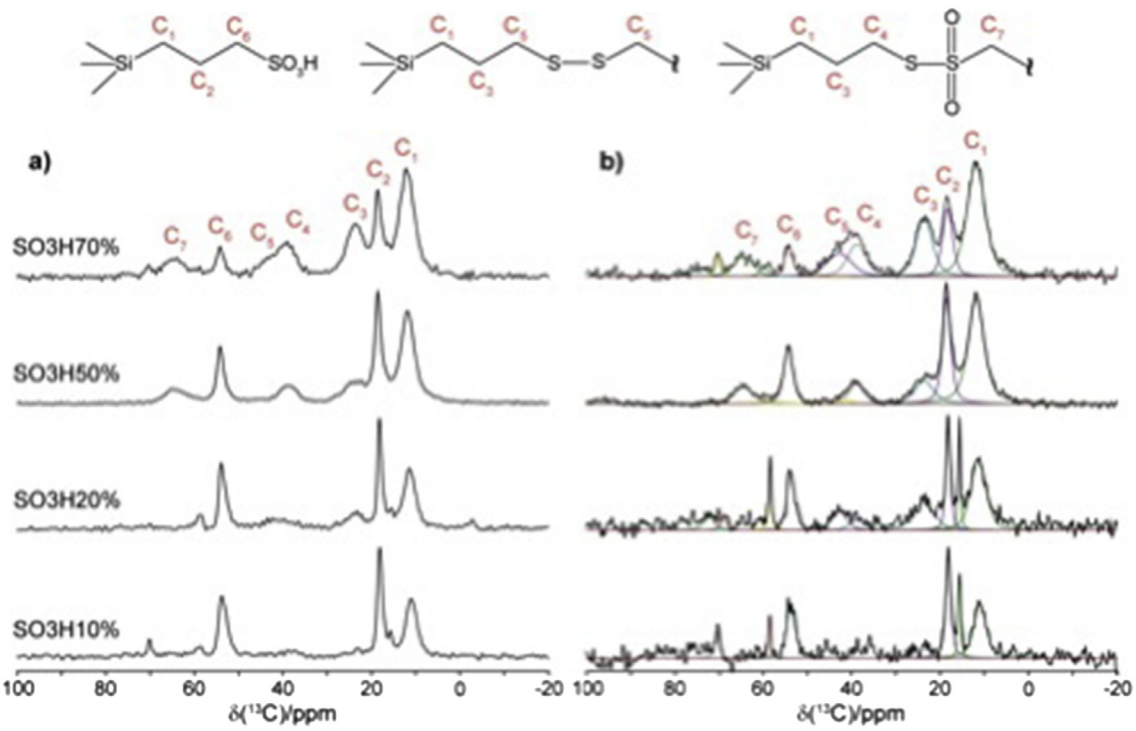

Fig. 8. ^{13}C NMR spectra recorded for pure SBA-15 and a series of propylsulfonic functionalized mesoporous silicas: a) ^{13}C(^{1}H) CP MAS experiments (contact time 2.5 ms); b) ^{13}C MAS experiments (recycle delay 30 s). The colored lines are the lineshape deconvolution components summarized in Table 3.

Table 3
Assignment of the ^{13}C MAS-NMR spectra (Fig. 8).

C site	δ_{CS} (ppm, ± 0.2)			
	SO3H10%	SO3H20%	SO3H50%	SO3H70%
Si–***CH$_2$***–CH_2–CH_2–X	11.0	11.3	11.8	11.8
CH_3–, PO units P123; ***CH$_3$***CH_2OH	15.6	15.6	–	–
Si–CH_2–***CH$_2$***–CH_2–SO_3H	18.1	18.1	18.4	18.2
Si–CH_2–***CH$_2$***–CH_2–S–S–		23.7	23.6	23.6
Si–CH_2–CH_2–***CH$_2$***–S–S(O_2)–			38.7	38.9
Si–CH_2–CH_2–***CH$_2$***–S–S–		41.4	41.2	42.8
Si–CH_2–CH_2–***CH$_2$***–SO_3H	53.7	53.8	54.3	54.2
CH_3***CH$_2$***OH	58.5	58.4	–	59.6
Si–CH_2–CH_2–CH_2–S–S(O_2)–***CH$_2$***–			64.6	64.5
–CH_2–, EO units P123	70.6	70.0	–	70.4
–CH_2–, PO units P123		72.4	–	74.6

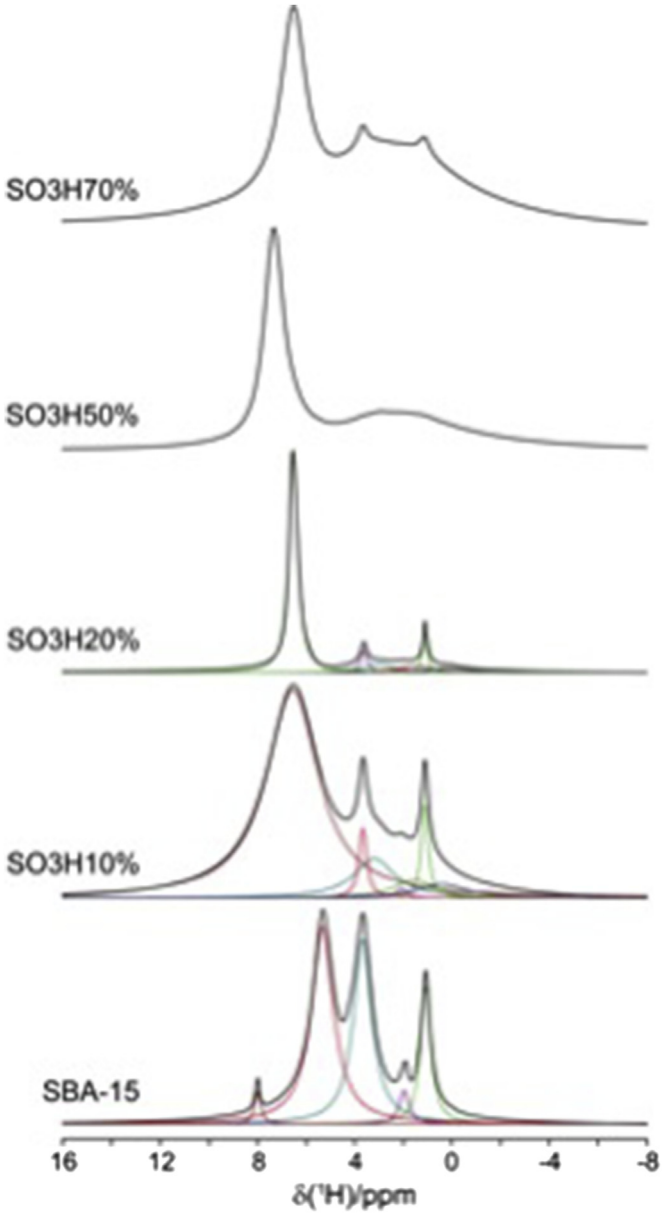

Fig. 9. ^1H single pulse MAS NMR spectra recorded for pure SBA-15 and several one-step propylsulfonic functionalized mesoporous silicas. The colored lines are line-shape deconvolution components (see also Table 4).

Table 4
Assignment of the ^1H MAS-NMR spectra (Fig. 9).

H site	δ_{CS} (ppm, ±0.2)		
	SBA-15	SO3H10%	SO3H20%
Si***CH$_2$***$CH_2$$CH_2$–X	–	0.4	0.1
CH_3 in PO units P123, CH_3CH_2**OH**	1.1	1.1	1.1
SiCH_2***CH$_2$***CH_2–X	–	1.5	1.5
isolated silanols	2.0	2.1	2.1
SiCH_2CH_2***CH$_2$***–SO_3H or –X	–	3.2	3.0
CH_2 in PO/EO units P123, CH_3***CH$_2$***OH	3.7	3.7	3.6
H-bonded silanols + coordinated water	5.3	6.6	6.5
–SO_3H + coordinated water	–	6.6	6.5
Impurity	8.0	–	–

structure in the 4–0 ppm range. The higher chemical shift of the main peak assigned to acidic protons mirrors the increased acidity of the SO_3H-groups [10,41]. Due to the formation of disulfide and thiosulfonate bridges, the number of non equivalent protons resonating in the 4–0 ppm drastically increases, making any deeper investigation impossible. A similar spectrum was recorded for the SO3H70% sample. However, two important differences should be noted: i) the peak due to the sulfonic acid protons is centered at 6.5 ppm, suggesting a decrease of the acidic strength to levels similar to that of low functionalized SO3H10% and SO3H20% samples; ii) in the broad lineshape at 4–0 ppm two sharp peaks centered at 3.7 and 1.1 ppm can be recognized, which are again assigned to the templating agent. Concerning the first point, we stressed that in the previous ^{13}C NMR section we quantified in 10–20% the conversion of –SH to $-SO_3H$ groups for this sample. As a consequence, an overall acidic strength similar to that of the SO3H10% and SO3H20% samples is consistent with the real amount of acidic moieties. For the second point, the relative large residue of Pluronic® can be explained with the formation of a disordered and not uniform mesoporous structure, where part of the template is trapped in closed pores, so that it cannot be removed during the post-synthesis ethanol washing.

4. Conclusions

SBA-15 silicas functionalized with propylsulfonic units were synthesized by one-step reaction between TEOS and MTPMS, in presence of Pluronic® and H_2O_2 as the oxidant. The compositional range of the $-SO_3H$ units was varied between 0 and 70 mol%, and a fair agreement between the nominal and actual concentration of the organic groups was obtained for each investigated sample.

The morphological and microstructural investigation on the hybrid systems describes a progressive loss of the typical SBA mesostructural order by increasing the sulfonation degree. In case of the SO3H50% sample, the hexagonal arrangement definitely

collapses. At low functionalization degrees (10 and 20 mol%) the samples show a monomodal pore size distribution, peaked around 6 nm, indicating a substantial retaining of the pristine SBA-15 honeycomb structure. In contrast, at higher functionalization degrees a bimodal pore size distribution, with maxima at 4 nm and 12 nm, is observed and this is an index of a different and more disordered structure. A gradual increase of the wall thickness also resulted as a consequence of the functionalization process, changing from 43 Å for SBA-15 to 73 Å for SO3H20%.

The multinuclear NMR study draws a picture of the distribution and fate of the sulfonic moieties into the silica network. ^{13}C and ^{1}H NMR spectra show that full conversion of the SH-groups to $-SO_3H$ ones is possible only at low functionalization degrees. In case of higher sulfonation degrees, in contrast, the formation of S–S bridges is a competitive mechanism, which becomes predominant in the sample SO3H70%, where only about 20% of the introduced organic moieties are actually oxidized. The ^{29}Si quantitative NMR spectra indicate a partial retaining of the SBA-15 original structure even at high $-SO_3H$ contents. This evidence can be likely justified by the presence of ordered inorganic mesoporous clusters, which are dispersed in a disordered hybrid network, where “broken” hexagonal cells and disulfide bridges are presumably located. In conclusion, functionalization degrees higher than 20 mol% lead to inhomogeneous materials, with poor mesoporous order and a lower than expected number of sulfonic moieties, due to S–S– bridges formation. A functionalization degree of 20 mol% is confirmed as the limiting stress that the SBA-15 honeycomb structure can stand before collapsing. On the other hand, a higher functionalization degree does not imply better reactivity for catalysis or other applications, such as fillers in ion-conducting membranes, due to disulfide bridges competitive mechanism, which can be also at the origin of the observed substantial decrease of specific surface area and mesoporous signature.

Finally, we think our paper can be of great interest for materials chemists, and can also pave the way for the set-up of new, and more powerful, strategies to extend the functionalization levels of mesoporous silicas well beyond the present limitations.

Acknowledgements

This work was done in the frame of the project financed by Italian Ministry of University and Research (MIUR) (PRIN 2010, 2010CYTWAW).

Appendix A. Supplementary data

Supplementary data related to this article can be found at http://dx.doi.org/10.1016/j.micromeso.2015.08.011.

References

[1] C.T. Kresge, M.E. Leonowicz, W.E. Roth, J.C. Vartuli, J.S. Beck, Nature 359 (1992) 710–712.
[2] J.S. Beck, J.C. Vartuli, W.J. Roth, M.E. Leonowicz, C.T. Kresge, K.D. Schmitt, C.T.-W. Chu, D.H. Olson, E.W. Sheppard, S.B. McCullen, J.B. Higgins, J.L.A. Schlenker, J. Am. Chem. Soc. 114 (1992) 10834–10843.
[3] D. Zhao, J. Feng, Q. Huo, N. Melosh, G.H. Frederickson, B.F. Chmelka, G.D. Stucky, Science 279 (1998) 548–552.
[4] D. Margolese, J.A. Melero, S.C. Christiansen, B.F. Chmelka, G.D. Stucky, Chem. Mater. 12 (2000) 2448–2459.
[5] S. Inagaki, S. Guan, T. Ohsuna, O. Terasaki, Nature 416 (2002) 304–307.
[6] A. Stein, J.B. Melde, R.C. Schroden, Adv. Mater. 12 (2000) 1403–1419.
[7] A.P. Wight, M.E. Davis, Chem. Rev. 102 (2002) 3589–3614.
[8] W.M. Van Rhijn, D.E. De Vos, B.F. Sels, W.D. Bossaert, P.A. Jacobs, Chem. Commun. (1998) 317–318.
[9] V. Dufaud, M.E. Davis, J. Am. Chem. Soc. 125 (2003) 9403–9413.
[10] R. Siegel, E. Domingues, R. De Sousa, F. Jérôme, C.M. Morais, N. Bion, P. Ferreira, L. Mafra, J. Mater. Chem. 22 (2012) 7412–7419.
[11] H.H.P. Yiu, P.A. Wright, J. Mater. Chem. 15 (2005) 3690–3700.
[12] S. Wang, Micropor. Mesopor. Mater. 117 (2008) 1–9.
[13] C. Sanchez, B. Julián, P. Belleville, M. Popall, J. Mater. Chem. 15 (2005) 3559–3592.
[14] X. Feng, G.E. Fryxell, L.-Q. Wang, A.Y. Kim, J. Liu, K.M. Kemner, Science 276 (1997) 923–926.
[15] E. De Canck, I. Ascoop, A. Sayari, P. Van der Voort, Phys. Chem. Chem. Phys. 15 (2013) 9792–9799.
[16] S. Fujita, K. Kamazawa, S. Yamamoto, M. Tyagi, T. Araki, J. Sugiyama, N. Hasegawa, M. Kawasumi, J. Phys. Chem. C 117 (2013) 8727–8736.
[17] N. Bibent, T. Charpentier, S. Devautour-Vinot, A. Mehdi, P. Gaveau, F. Henn, G. Silly, Eur. J. Inorg. Chem. 2013 (2013) 2350–2361.
[18] Y.-C. Pan, H.-H.G. Tsai, J.-C. Jiang, C.-C. Kao, T.-L. Sung, P.-J. Chiu, D. Saikia, J.-H. Chang, H.-M. Kao, J. Phys. Chem. C 116 (2011) 1658–1669.
[19] P. Shah, V. Ramaswamy, Micropor. Mesopor. Mater. 114 (2008) 270–280.
[20] S. Chytil, L. Haugland, E.A. Blekkan, Micropor. Mesopor. Mater. 111 (2008) 134–142.
[21] Y.-F. Feng, X.-Y. Yang, Y. Di, Y.-C. Du, Y.-L. Zhang, F.-S. Xiao, J. Phys. Chem. B 110 (2006) 14142–14147.
[22] D. Das, J.-F. Lee, S. Cheng, Chem. Commun. (2001) 2178–2179.
[23] L.M. Yang, Y.J. Wang, G.S. Luo, Y.Y. Dai, Micropor. Mesopor. Mater. 84 (2005) 275–282.
[24] X. Zhuoying, B. Ling, H. Suwen, Z. Cun, Z. Yuanjin, G. Zhong-Ze, J. Am. Chem. Soc. 136 (2014) 1178–1181.
[25] G. Morales, G. Athens, B.F. Chmelka, R. van Grieken, J.A. Melero, J. Catal. 254 (2008) 205–217.
[26] I.B. Shir, S. Kababya, A. Schmidt, J. Phys. Chem. C 116 (2012) 9691–9702.
[27] G. Paul, S. Steuernagel, H. Koller, Chem. Commun. (2007) 5194–5196.
[28] A.S. Cattaneo, S. Bracco, A. Comotti, M. Galimberti, P. Sozzani, H. Eckert, J. Phys. Chem. C 115 (2011) 12517–12529.
[29] S. Brunauer, P.H. Emmett, E. Teller, J. Am. Chem. Soc. 60 (1938) 309–319.
[30] E.P. Barrett, L.G. Joyner, P.P. Halenda, J. Am. Chem. Soc. 73 (1951) 373–380.
[31] D. Massiot, F. Fayon, M. Capron, I. King, S. Le Calvé, B. Alonso, J.O. Durand, B. Bujoli, Z. Gan, G. Hoatson, Magn. Reson. Chem. 40 (2002) 70–76.
[32] M.D. Abramoff, P.J. Magalhaes, S.J. Ram, Biophotonics Int. 11 (2004) 36–42.
[33] W.S. Rasband, J. Image, U.S. National Institutes of Health, Bethesda, MD, USA, 1997–2001. http://imagej.nih.gov/ij/.
[34] Z. Luan, E.M. Maes, P.A.W. van der Heide, D. Zhao, R.S. Czernuszewicz, L. Kevan, Chem. Mater. 11 (1999) 3680–3686.
[35] N. Das, H. Eckert, H. Hu, I.E. Wachs, J.F. Walzer, F.J. Feher, J. Phys. Chem. 97 (1993) 8240–8243.
[36] X. Wang, K.S.K. Lin, J.C.C. Chan, S. Cheng, J. Phys. Chem. B 109 (2005) 1763–1769.
[37] K. Grzechnik, K. Rutkowski, Z. Mielke, J. Mol. Struct. 1009 (2012) 96–102.
[38] K.S.W. Sing, D.H. Everett, R.A.W. Haul, L. Moscou, R.A. Pierotti, J. Rouquerol, T. Siemieniewska, Pure Appl. Chem. 57 (1985) 603–619.
[39] M. Kruk, M. Jaroniec, C.H. Ko, R. Ryoo, Chem. Mater. 12 (2000) 1961–1968.
[40] K.J.M. Mac Kenzie, M.E. Smith, Multinuclear Solid-state Nuclear Magnetic Resonance of Inorganic Materials, Pergamon, 2002, p. 201 (Chapter 4).
[41] R. Kanthasamy, I.K. Mbaraka, B.H. Shanks, S.C. Larsen, Appl. Magn. Reson. 32 (2007) 513–526.
[42] X. Wang, S. Cheng, J.C.C. Chan, J. Phys. Chem. C 111 (2007) 2156–2164.
[43] H.-H.G. Tsai, P.-J. Chiu, G.L. Jheng, C.-C. Ting, Y.-C. Pan, H.-M. Kao, J. Coll. Inter. Sci. 359 (2011) 86–94.
[44] I. Dìaz, C. Márquez-Alvarez, F. Mohino, J. Pérez-Pariente, E. Sastre, J. Catal. 193 (2000) 283–294.
[45] C.-M. Yang, B. Zibrowius, W. Schmidt, F. Schüth, Chem. Mater. 16 (2004) 2918–2925.
[46] B. Grünberg, T. Emmler, E. Gedat, I. Shenderovich, G.H. Findenegg, H.-H. Limbach, G. Buntkowsky, Chem. Eur. J. 10 (2004) 5689–5696.
[47] K. Flodström, H. Wennerström, V. Alfredsson, Langmuir 20 (2004) 680–688.